On the Limits of Single Anchor Localization: Near-Field vs. Far-Field

Don-Roberts Emenonye, Harpreet S. Dhillon, and R. Michael Buehrer

***Abstract*—It is well known that a single anchor can be used to determine the position and orientation of an agent communicating with it. However, it is not clear what information about the anchor or the agent is necessary to perform this localization, especially when the agent is in the near-field of the anchor. Hence, in this paper, to investigate the limits of localizing an agent with some uncertainty in the anchor location, we consider a wireless link consisting of source and destination nodes. More specifically, we present a Fisher information theoretical investigation of the possibility of estimating different combinations of the source and destination's position and orientation from the signal received at the destination. To present a comprehensive study, we perform this Fisher information theoretic investigation under both the near and far field propagation models. One of the key insights is that while the source or destination's 3D orientation can be jointly estimated with the source or destination's 3D position in the near-field propagation regime, only the source or destination's 2D orientation can be jointly estimated with the source or destination's 2D position in the far-field propagation regime. Also, a simulation of the FIM indicates that in the near-field, we can estimate the source's 3D orientation angles with no beamforming, but in the far-field, we can not estimate the source's 2D orientation angles when no beamforming is employed.**

***Index Terms*—6G localization, anchor uncertainty, far-field, near-field, FIM.**

I. Introduction

Recently, due to the ubiquitous deployment of multi-antenna base stations, single-anchor localization has been proposed and studied with [1], [2] and without a reconfigurable intelligent surface (RIS) [3], [4], [5]. Localization is usually performed under the assumption that the anchor location (position and orientation) is perfectly known [6]. However, in practical systems, this assumption might not hold. For example, in scenarios where unmanned aerial vehicles (UAV) act as anchors, there could be inherent uncertainty in the locations of the UAVs [7]. Another example involves localization using RISs. RISs are being considered to aid localization by acting as virtual anchors; however, their ubiquitous deployment means that their locations can change (e.g., when they are placed on movable objects), resulting in uncertainty in their locations. Lastly, in indoor localization systems, the locations of the indoor anchors can easily be disturbed after deployment. Hence, in this paper, to investigate localization with anchor uncertainty, we present a Fisher information view of estimating different combinations of a source and destination's position and orientation under the near and far field propagation regimes.

D.-R. Emenonye, H. S. Dhillon and R. M. Buehrer are with Wireless@VT, Bradley Department of Electrical and Computer Engineering, Virginia Tech, Blacksburg, VA, 24061, USA. Email: {donroberts, hdhillon, rbuehrer}@vt.edu. The support of the US National Science Foundation (Grants ECCS-2030215 and CNS-2107276) is gratefully acknowledged.

A. Prior Art

Prior literature on single-anchor localization involves deriving the fundamental limits for the accuracy achievable in estimating the position and orientation of an agent [1]. These bounds are extended to the case of 3D localization of an agent in [2]. In [8], the amount of information in the non-line of sight (NLOS) paths and their usefulness for localization is analyzed. The bounds of single-anchor localization with a RIS have been studied in [3]. These bounds are extended to account for near-field propagation in [4], [5]. In the context of anchor state uncertainty, localization has been investigated with and without a RIS. In [9], the positioning problem in the presence of anchor uncertainty is studied, the resulting non-convex optimization problem is relaxed to a second-order cone programming problem, and semidefinite programming is applied. The authors in [10] derive the geometric dilution of precision in the presence of anchor position uncertainty, and a trade-off is made between range errors and position errors by applying the modified spring mass method. The anchor position offset and the agent's position are estimated in [11] using the signal strength of the received signals. In [12], a rigorous investigation of the impact of anchor uncertainty on received signal strength-based localization techniques is presented. Uncertainties are considered in the case of RIS-assisted localization in [3], [4]. While the prior art primarily includes robust algorithms to handle uncertainty in anchors' position, a comprehensive Fisher information-based analysis on the estimation of the anchor orientation has yet to be studied. It is important to note the anchor orientation is particularly important as the localization of agents is now being considered using a single anchor with large number of antennas. Moreover, the effect of anchor location uncertainty has not been investigated under the near-field propagation regime.

B. Contributions

In this paper, through the Fisher information matrix (FIM), we present a theoretical investigation of the limits of single-anchor localization by determining the combinations of positions and orientations of the source and destination nodes that can be estimated in the near and far field propagation regimes. Further, using the FIM, we present a lower bound for the source orientation and destination position accuracy. One key result from the FIM-based analysis is that in the

near-field, the source or destination's 3D orientations can be estimated jointly with either the source or destination's 3D positions. Also, in the far-field, the source or destination's 2D orientations can be estimated jointly with either the source or destination's 2D positions. Another result is that while the presence of a beamforming matrix is not required in the near-field to estimate the source's 3D orientation angles, a beamforming matrix is required in the far-field to estimate the source's 2D orientation angles.

Notation: the transpose operator is $(\cdot)^{\mathrm{T}}$; the hermitian transpose operator is $(\cdot)^{\mathrm{H}}$; the submatrix in the matrix $\boldsymbol{V}$, with rows in the range, $g_1 : v_1$, and the columns in the range $g_2 : v_2$ is extracted using the operation $[\boldsymbol{V}]_{[g_1:v_1,g_2:v_2]}$; $\mathrm{Tr}(\cdot)$ is the matrix trace operator; $\|\cdot\|$ denotes the Euclidean norm ; the positive definiteness of a matrix is characterized by $\succ$; the first derivative operator is ∇ ; the expectation operator with respect to the random vector $\boldsymbol{v}$ is $\mathbb{E}_{\boldsymbol{v}}\{\cdot\}$.

II. System Model

We consider a source with its centroid located at $\boldsymbol{p}_B = [x_B, y_B, z_B]^{\mathrm{T}}$, and its b^{th} antenna element located at $\boldsymbol{s}_b = [x_b, y_b, z_b]^{\mathrm{T}}$. The location of the centroid is defined with respect to the global origin, while the location specified by $\boldsymbol{s}_b$ is defined with respect to $\boldsymbol{p}_B$.

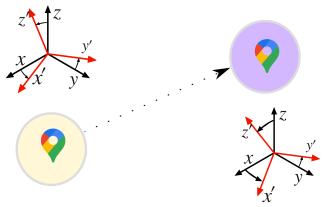

Figure 1. An illustration showing a source communicating with a destination.

This point $\boldsymbol{s}_b$ can also be written as $\boldsymbol{s}_b = \boldsymbol{Q}_B \tilde{\boldsymbol{s}}_b$, where $\tilde{\boldsymbol{s}}_b = [\tilde{x}_b, \tilde{y}_b, \tilde{z}_b]^{\mathrm{T}}$ is the previously known position of the antenna coordinate with respect to $\boldsymbol{p}_B$ before an orientation offset, $\boldsymbol{\Phi}_B = [\alpha_B, \psi_B, \varphi_B]^{\mathrm{T}}$. The subsequent 3D orientation matrix is defined as $\boldsymbol{Q}_B$ [13]. There are N_B antennas at the source, and each antenna can be described with respect to the global origin as $\boldsymbol{p}_b = \boldsymbol{p}_B + \boldsymbol{s}_b$. The destination is located at $\boldsymbol{p}_U = [x_U, y_U, z_U]^{\mathrm{T}}$, and its u^{th} antenna element is located at $\boldsymbol{s}_u = [x_u, y_u, z_u]^{\mathrm{T}}$. The corresponding vectors, $\boldsymbol{p}_U$, $\boldsymbol{s}_u$, $\tilde{\boldsymbol{s}}_u$ and $\boldsymbol{p}_u$ have similar definitions as the corresponding source's vectors. Note that the orientation angles and the matrix related to the destination are denoted by $\boldsymbol{\Phi}_U$ and $\boldsymbol{Q}_U$, respectively. The position of the destination's centroid located at $\boldsymbol{p}_U$ can be described in relation to the position of the source's centroid located at $\boldsymbol{p}_B$ as $\boldsymbol{p}_U = \boldsymbol{p}_B + d_{BU}\boldsymbol{\Delta}_{BU}$, where d_{BU} is the distance from point $\boldsymbol{p}_B$ to point $\boldsymbol{p}_U$ and $\boldsymbol{\Delta}_{BU}$ is the corresponding unit direction vector $\boldsymbol{\Delta}_{BU} = [\cos\phi_{BU}\sin\theta_{BU}, \sin\phi_{BU}\sin\theta_{BU}, \cos\theta_{BU}]^{\mathrm{T}}$. All points defined locally that describe the location of elements on the source antenna array with respect to the source's centroid can be written in the matrix form as $\boldsymbol{S}_B = [\boldsymbol{s}_1, \boldsymbol{s}_2, \cdots, \boldsymbol{s}_{N_B}]$. Similarly, the points defined locally that describe the location of elements on the destination antenna array with respect to the destination's centroid can be written in the matrix form as $\boldsymbol{S}_U = [\boldsymbol{s}_1, \boldsymbol{s}_2, \cdots, \boldsymbol{s}_{N_U}]$. Matrices $\tilde{\boldsymbol{S}}_B$ and $\tilde{\boldsymbol{S}}_U$ can be described similarly, by collecting the appropriate vectors $\tilde{\boldsymbol{s}}_b$ and $\tilde{\boldsymbol{s}}_u$.

A. Signal Model

The communication from the source to the destination is achieved through the transmission of T symbols from the source with N_B transmit antennas to the destination with N_U receive antennas. During each transmission, the source precodes a deterministic data stream (i.e., a training sequence), $\boldsymbol{x} \in \mathcal{C}^{N_D \times 1}$, to the N_B transmit antennas with a beamforming matrix $\boldsymbol{F}_t \in \mathcal{C}^{N_B \times N_D}$ under a unit power constraint. The signal received during the t^{th} transmission is

$$\boldsymbol{y}_t = \boldsymbol{H}\boldsymbol{F}_t\boldsymbol{x} + \boldsymbol{n}_t, = \boldsymbol{\mu}_t + \boldsymbol{n}_t. \tag{1}$$

In the above equation, $\boldsymbol{\mu}_t$ is the noise-free part (useful part) of the signal, and $\boldsymbol{n}_t \sim \mathcal{CN}(0, N_0)$ represents the thermal noise local to the destination's antenna array. Considering narrowband transmissions, the element in the u^{th} row and b^{th} column of the channel matrix $\boldsymbol{H}$ is $[\boldsymbol{H}]_{[u,b]} = \beta e^{-j2\pi f_c \tau_{bu}}$[1]. Here, $\beta = \beta_{\mathrm{R}} + j\beta_{\mathrm{I}}$ is the complex path gain, f_c is the operating frequency, and τ_{bu} is the propagation delay from the b^{th} transmit antenna located at $\boldsymbol{p}_b$ on the source's antenna array to the receive antenna located at $\boldsymbol{p}_u$ on the destination's antenna array. Now, the signal received at the destination's u^{th} receive antenna during the t^{th} transmission is

$$\boldsymbol{y}_{t,u} = \sum_{b=1}^{N_B}\sum_{d=1}^{N_D}[\boldsymbol{F}_t]_{[b,d]}[\boldsymbol{x}]_{[d]}[\boldsymbol{H}]_{[u,b]} + \boldsymbol{n}_t. \tag{2}$$

The definition of the delay given as $\tau_{bu} = \frac{\|\boldsymbol{p}_u - \boldsymbol{p}_b\|}{c}$ incorporates any potential spherical curvature wavefront present in the signal received at the destination. When the destination experiences substantial wavefront curvature, it is said to be located within the near-field propagation regime. It is important to note that at sufficiently larger distances between the destination and the source, the spherical wavefront can be approximated by a plane wave. With this plane wave approximation, the delay can be approximated as $\tau_{bu} = \tau_{BU} + \Delta_{BU}^{\mathrm{T}}(\boldsymbol{s}_u - \boldsymbol{s}_b)/c$. When this approximation holds, the destination is said to be located within the far-field propagation regime. The boundary that defines the near and far field propagation regime is called the Fraunhofer distance. This Fraunhofer distance can be computed as $d_{\mathrm{f}} = 2D^2/\lambda$ with λ indicating the wavelength of the signal and D the maximum diameter among the source and destination surface diameters [4]. While, (1) and (2) adequately represent the signals received in the near-field, an approximation of signals received in the far-field can be written as

$$\boldsymbol{y}_t = \beta\boldsymbol{a}_{UB}(\Delta_{BU})\boldsymbol{a}_{BU}^{\mathrm{H}}(\Delta_{BU})e^{-j2\pi f_c\tau_{BU}}\boldsymbol{F}_t\boldsymbol{x} + \boldsymbol{n}_t, \tag{3}$$

where $\boldsymbol{a}_{BU}(\Delta_{BU}) = e^{-j2\frac{\pi}{\lambda}\boldsymbol{S}_B^{\mathrm{T}}\Delta_{BU}}$ and $\boldsymbol{a}_{UB}(\Delta_{BU}) = e^{-j2\frac{\pi}{\lambda}\boldsymbol{S}_U^{\mathrm{T}}\Delta_{BU}}$.

[1]The near-field model still needs to be standardized. In some papers, the complex path gains vary across the destination antenna array.

B. Source and Destination Position and Orientation Estimation

In this letter, we provide the different combinations of source and destination position and orientation that can be estimated through the signals received across the N_U antennas during the T transmissions. We determine this by evaluating the FIM under the following parameterizations: case I) $\boldsymbol{\eta} = [\boldsymbol{p}_U, \boldsymbol{\Phi}_U, \boldsymbol{\beta}]^{\mathrm{T}}$, case II) $\boldsymbol{\eta} = [\boldsymbol{p}_U, \boldsymbol{\Phi}_B, \boldsymbol{\beta}]^{\mathrm{T}}$, case III) $\boldsymbol{\eta} = [\boldsymbol{p}_B, \boldsymbol{\Phi}_U, \boldsymbol{\beta}]^{\mathrm{T}}$, and case IV) $\boldsymbol{\eta} = [\boldsymbol{p}_B, \boldsymbol{\Phi}_B, \boldsymbol{\beta}]^{\mathrm{T}}$. Here, $\boldsymbol{\beta} = [\beta_{\mathrm{R}}, \beta_{\mathrm{I}}]^{\mathrm{T}}$. Note that the location parameters for each individual case can be collected into the vector $\boldsymbol{\zeta}$. The FIM computations are carried under three scenarios: i) far-field model with beamforming, ii) near-field model with no beamforming, and iii) near-field model with beamforming. Note that the case for using the far-field model with identity beamforming matrices across the T transmissions is not possible. This is because the joint estimation of the source orientation, $\boldsymbol{\Phi}_B$, and $\boldsymbol{\beta}$ is not feasible under this condition (see Appendix A).

III. Information in the Received signal

To analyze the amount of location information present in the received signal, we introduce the mathematical definition of the FIM for an unknown parameter vector, $\boldsymbol{\eta}$, in the following definition.

Definition 1. *Based on a set of observations* $\mathbf{y}$*, the Fisher information of a parameter vector,* $\boldsymbol{\eta}$*, is written as* $\mathbf{J}_{\boldsymbol{\eta}} \triangleq -\mathbb{E}_{\mathbf{y}}\left[\frac{\partial^2 \ln \chi(\mathbf{y}|\boldsymbol{\eta})}{\partial \boldsymbol{\eta} \partial \boldsymbol{\eta}^{\mathrm{T}}}\right]$ *where* $\mathbb{E}_{\nu}$ *is expectation taken over the random variable* ν*,* $\chi(\mathbf{y}|\boldsymbol{\eta})$ *is the likelihood of* $\boldsymbol{y}$ *conditioned on* $\boldsymbol{\eta}$*. We note that the error covariance matrix of an unbiased estimate,* $\hat{\boldsymbol{\eta}}$*, of an unknown parameter vector,* $\boldsymbol{\eta}$ *satisfies the following information inequality* $\mathbb{E}_{\boldsymbol{y}}\left\{(\hat{\boldsymbol{\eta}} - \boldsymbol{\eta})(\hat{\boldsymbol{\eta}} - \boldsymbol{\eta})^{\mathrm{T}}\right\} \succeq \mathbf{J}_{\boldsymbol{\eta}}^{-1}$.

The FIM for the parameter vector $\boldsymbol{\eta} = [\boldsymbol{p}_U, \boldsymbol{\Phi}_B, \boldsymbol{\beta}]^{\mathrm{T}}$ has the following structure

$$\mathbf{J}_{\boldsymbol{\eta}} \triangleq \begin{bmatrix} \mathbf{J}_{\boldsymbol{p}_U \boldsymbol{p}_U} & \mathbf{J}_{\boldsymbol{p}_U \boldsymbol{\Phi}_B} & \mathbf{J}_{\boldsymbol{p}_U \boldsymbol{\beta}_{\mathrm{R}}} & \mathbf{J}_{\boldsymbol{p}_U \boldsymbol{\beta}_{\mathrm{I}}} \\ \mathbf{J}_{\boldsymbol{\Phi}_B \boldsymbol{p}_U} & \mathbf{J}_{\boldsymbol{\Phi}_B \boldsymbol{\Phi}_B} & \mathbf{J}_{\boldsymbol{\Phi}_B \boldsymbol{\beta}_{\mathrm{R}}} & \mathbf{J}_{\boldsymbol{\Phi}_B \boldsymbol{\beta}_{\mathrm{I}}} \\ \mathbf{J}_{\boldsymbol{\beta}_{\mathrm{R}} \boldsymbol{p}_U} & \mathbf{J}_{\boldsymbol{\beta}_{\mathrm{R}} \boldsymbol{\Phi}_B} & \mathbf{J}_{\boldsymbol{\beta}_{\mathrm{R}} \boldsymbol{\beta}_{\mathrm{R}}} & \mathbf{J}_{\boldsymbol{\beta}_{\mathrm{R}} \boldsymbol{\beta}_{\mathrm{I}}} \\ \mathbf{J}_{\boldsymbol{\beta}_{\mathrm{I}} \boldsymbol{p}_U} & \mathbf{J}_{\boldsymbol{\beta}_{\mathrm{I}} \boldsymbol{\Phi}_B} & \mathbf{J}_{\boldsymbol{\beta}_{\mathrm{I}} \boldsymbol{\beta}_{\mathrm{R}}} & \mathbf{J}_{\boldsymbol{\beta}_{\mathrm{I}} \boldsymbol{\beta}_{\mathrm{I}}} \end{bmatrix} \in \mathcal{R}^{8 \times 8}. \tag{4}$$

The submatrices in the above matrix can be computed using $\mathbf{J}_{\boldsymbol{\eta}_{\mathbf{v}_1} \boldsymbol{\eta}_{\mathbf{v}_2}} \triangleq \frac{2}{\sigma^2} \sum_{t=1}^{T} \Re\left\{ \frac{\partial \boldsymbol{\mu}_t^{\mathrm{H}}}{\partial \boldsymbol{\eta}_{\mathbf{v}_1}} \frac{\partial \boldsymbol{\mu}_t}{\partial \boldsymbol{\eta}_{\mathbf{v}_2}} \right\}$ where $\boldsymbol{\eta}_{\mathbf{v}_1} \in \boldsymbol{\eta}$, $\boldsymbol{\eta}_{\mathbf{v}_2} \in \boldsymbol{\eta}$ are both dummy variables, and $1/\sigma^2$ is the SNR which incorporates the pathloss and composite noise power. The required first derivatives are presented in the following sections.

A. First Derivatives under the Far-Field Model

The first derivative of the useful part of the received signal with respect to $\nu \in [\boldsymbol{p}_B, \boldsymbol{p}_U]$ under the far-field model is

$$\nabla_{\nu} \boldsymbol{\mu}_{t,u} = \beta e^{-j2\frac{\pi}{\lambda} \boldsymbol{s}_u^{\mathrm{T}} \Delta_{BU}} \boldsymbol{a}_{BU}^{\mathrm{H}}(\Delta_{BU}) \boldsymbol{K}_{\nu} e^{-j2\pi f_c \tau_{BU}} \boldsymbol{F}_t \boldsymbol{x},$$

where $\boldsymbol{K}_{\nu}$ is expressed in (5). The first derivatives of the useful part of the received signal with respect to $\nu \in \boldsymbol{\Phi}_B$ and $\nu \in \boldsymbol{\Phi}_U$ under the far-field model are

$$\nabla_{\nu} \boldsymbol{\mu}_t = \beta \tilde{\boldsymbol{P}}_{\nu} \boldsymbol{a}_{UB}(\Delta_{BU}) \boldsymbol{a}_{BU}^{\mathrm{H}}(\Delta_{BU}) e^{-j2\pi f_c \tau_{BU}} \boldsymbol{F}_t \boldsymbol{x},$$

$$\nabla_{\nu} \boldsymbol{\mu}_{t,u} = \beta e^{-j2\frac{\pi}{\lambda} \boldsymbol{s}_u^{\mathrm{T}} \Delta_{BU}} \boldsymbol{a}_{BU}^{\mathrm{H}}(\Delta_{BU}) \boldsymbol{P}_{\nu} e^{-j2\pi f_c \tau_{BU}} \boldsymbol{F}_t \boldsymbol{x},$$

respectively, where

$$\tilde{\boldsymbol{P}}_{\nu} = \mathrm{diag}\left[-\frac{j2\pi}{\lambda} (\nabla_{\nu} \boldsymbol{S}_u)^{\mathrm{T}} \left[\frac{\boldsymbol{p}_U - \boldsymbol{p}_B}{d_{BU}} \right] \right],$$

$$\boldsymbol{P}_{\nu} = \mathrm{diag}\left[\frac{j2\pi}{\lambda} \left[\frac{\boldsymbol{p}_U - \boldsymbol{p}_B}{d_{BU}} \right]^{\mathrm{T}} \nabla_{\nu} \boldsymbol{S}_B \right].$$

Also, $\nabla_{\boldsymbol{\Phi}_B} \boldsymbol{S}_B = \nabla_{\boldsymbol{\Phi}_B} \boldsymbol{Q}_B \tilde{\boldsymbol{S}}_B$ and $\nabla_{\boldsymbol{\Phi}_U} \boldsymbol{S}_U = \nabla_{\boldsymbol{\Phi}_U} \boldsymbol{Q}_U \tilde{\boldsymbol{S}}_U$. Finally, the first derivative of the useful part of the received signal with respect to complex path gain under the far-field model is $\nabla_{\boldsymbol{\beta}_{\mathrm{R}}} \boldsymbol{\mu}_t = \boldsymbol{a}_{UB}(\Delta_{BU}) \boldsymbol{a}_{BU}^{\mathrm{H}}(\Delta_{BU}) \boldsymbol{F}_t \boldsymbol{x} e^{-j2\pi f_c \tau_{BU}}$, $\nabla_{\boldsymbol{\beta}_{\mathrm{I}}} \boldsymbol{\mu}_t = j \boldsymbol{a}_{UB}(\Delta_{BU}) \boldsymbol{a}_{BU}^{\mathrm{H}}(\Delta_{BU}) \boldsymbol{F}_t \boldsymbol{x} e^{-j2\pi f_c \tau_{BU}}$[2]. The above first derivatives are used to compute the submatrices with a similar structure as that shown in (4) when the far-field model is used.

B. First Derivatives under the Near-Field Model

The first derivatives of the useful part of the received signal with respect to $\boldsymbol{\eta}$ under the near-field model are

$$\nabla_{\boldsymbol{p}_U} \boldsymbol{\mu}_{t,u} = (-j2\pi f_c)\beta \sum_{b=1}^{N_B} \nabla_{\boldsymbol{p}_U} \tau_{bu} \sum_{d=1}^{N_D} [\boldsymbol{F}_t]_{[b,d]} [\boldsymbol{x}]_{[d]} e^{-j2\pi f_c \tau_{bu}},$$

$$\nabla_{\boldsymbol{p}_B} \boldsymbol{\mu}_{t,u} = (-j2\pi f_c)\beta \sum_{b=1}^{N_B} \nabla_{\boldsymbol{p}_B} \tau_{bu} \sum_{d=1}^{N_D} [\boldsymbol{F}_t]_{[b,d]} [\boldsymbol{x}]_{[d]} e^{-j2\pi f_c \tau_{bu}},$$

$$\nabla_{\boldsymbol{\Phi}_U} \boldsymbol{\mu}_{t,u} = (-j2\pi f_c)\beta \sum_{b=1}^{N_B} \nabla_{\boldsymbol{\Phi}_U} \tau_{bu} \sum_{d=1}^{N_D} [\boldsymbol{F}_t]_{[b,d]} [\boldsymbol{x}]_{[d]} e^{-j2\pi f_c \tau_{bu}},$$

$$\nabla_{\boldsymbol{\Phi}_B} \boldsymbol{\mu}_{t,u} = (-j2\pi f_c)\beta \sum_{b=1}^{N_B} \nabla_{\boldsymbol{\Phi}_B} \tau_{bu} \sum_{d=1}^{N_D} [\boldsymbol{F}_t]_{[b,d]} [\boldsymbol{x}]_{[d]} e^{-j2\pi f_c \tau_{bu}}.$$

$$\nabla_{\boldsymbol{\beta}_{\mathrm{R}}} \boldsymbol{\mu}_{t,u} = \sum_{b=1}^{N_B} \sum_{d=1}^{N_D} [\boldsymbol{F}_t]_{[b,d]} [\boldsymbol{x}]_{[d]} e^{-j2\pi f_c \tau_{bu}},$$

$$\nabla_{\boldsymbol{\beta}_{\mathrm{I}}} \boldsymbol{\mu}_{t,u} = j \sum_{b=1}^{N_B} \sum_{d=1}^{N_D} [\boldsymbol{F}_t]_{[b,d]} [\boldsymbol{x}]_{[d]} e^{-j2\pi f_c \tau_{bu}}.$$

Here, $\nabla_{\boldsymbol{p}_B} \tau_{bu} = \nabla_{\boldsymbol{p}_B} d_{bu}/c$, $\nabla_{\boldsymbol{p}_U} \tau_{bu} = \nabla_{\boldsymbol{p}_U} d_{bu}/c$, $\nabla_{\boldsymbol{\Phi}_U} \tau_{bu} = \nabla_{\boldsymbol{\Phi}_U} d_{bu}/c$, $\nabla_{\boldsymbol{\Phi}_B} \tau_{bu} = \nabla_{\boldsymbol{\Phi}_B} d_{bu}/c$, $\nabla_{\boldsymbol{p}_B} d_{bu} = -\frac{\boldsymbol{p}_u - \boldsymbol{p}_b}{d_{bu}}$, $\nabla_{\boldsymbol{p}_U} d_{bu} = \frac{\boldsymbol{p}_u - \boldsymbol{p}_b}{d_{bu}}$, $\nabla_{\boldsymbol{\Phi}_B} d_{bu} = -\frac{(\boldsymbol{p}_u - \boldsymbol{p}_b)^{\mathrm{T}}}{d_{bu}} (\nabla_{\boldsymbol{\Phi}_B} \boldsymbol{Q}_B \tilde{\boldsymbol{s}}_b)$, and $\nabla_{\boldsymbol{\Phi}_U} d_{bu} = \frac{(\boldsymbol{p}_u - \boldsymbol{p}_b)^{\mathrm{T}}}{d_{bu}} (\nabla_{\boldsymbol{\Phi}_U} \boldsymbol{Q}_U \tilde{\boldsymbol{s}}_u)$. The above first derivatives are used to compute the submatrices with a similar structure as that shown in (4) when the near-field model is used. After computing $\mathbf{J}_{\boldsymbol{\eta}}$, to focus on the available information concerning the location parameters, we present a mathematical description of the EFIM.

[2]The FIM is obtained by substituting the first derivatives into $\mathbf{J}_{\boldsymbol{\eta}_{\mathbf{v}_1} \boldsymbol{\eta}_{\mathbf{v}_2}} \triangleq \frac{2}{\sigma^2} \sum_{t=1}^{T} \Re\left\{ \frac{\partial \boldsymbol{\mu}_t^{\mathrm{H}}}{\partial \boldsymbol{\eta}_{\mathbf{v}_1}} \frac{\partial \boldsymbol{\mu}_t}{\partial \boldsymbol{\eta}_{\mathbf{v}_2}} \right\}$.

$$\boldsymbol{K}_{\nu} = \text{diag}\bigg[-\frac{j2\pi}{\lambda}\bigg(\boldsymbol{s}_u^{\mathrm{T}} \nabla_{\nu}\bigg[\frac{\boldsymbol{p}_U - \boldsymbol{p}_B}{d_{BU}}\bigg] - \nabla_{\nu}\bigg[\frac{\boldsymbol{p}_U - \boldsymbol{p}_B}{d_{BU}}\bigg]^{\mathrm{T}} \boldsymbol{S}_B + \nabla_{\nu} d_{BU}\bigg)\bigg], \tag{5}$$

$$\nabla_{\boldsymbol{p}_B} d_{BU} = -1 \times \bigg[\frac{\boldsymbol{p}_U - \boldsymbol{p}_B}{d_{BU}}\bigg], \;\; \nabla_{\boldsymbol{p}_B}\bigg[\frac{\boldsymbol{p}_U - \boldsymbol{p}_B}{d_{BU}}\bigg] = \frac{-d_{BU} - (\boldsymbol{p}_U - \boldsymbol{p}_B)\nabla_{\boldsymbol{p}_U} d_{BU}}{d_{BU}^2}, \tag{6}$$

$$\nabla_{\boldsymbol{p}_U} d_{BU} = \bigg[\frac{\boldsymbol{p}_U - \boldsymbol{p}_B}{d_{BU}}\bigg], \;\; \nabla_{\boldsymbol{p}_U}\bigg[\frac{\boldsymbol{p}_U - \boldsymbol{p}_B}{d_{BU}}\bigg] = \frac{d_{BU} - (\boldsymbol{p}_U - \boldsymbol{p}_B)\nabla_{\boldsymbol{p}_U} d_{BU}}{d_{BU}^2}. \tag{7}$$

Definition 2. *If the FIM of a parameter* $\boldsymbol{\eta} = [\boldsymbol{\eta}_1^{\mathrm{T}} \;\; \boldsymbol{\eta}_2^{\mathrm{T}}]^{\mathrm{T}}$ *is specified by*

$$\mathbf{J}_{\boldsymbol{\eta}} = \begin{bmatrix} \mathbf{J}_{\boldsymbol{\eta}_1\boldsymbol{\eta}_1} & \mathbf{J}_{\boldsymbol{\eta}_1\boldsymbol{\eta}_2} \\ \mathbf{J}_{\boldsymbol{\eta}_1\boldsymbol{\eta}_2}^{\mathrm{T}} & \mathbf{J}_{\boldsymbol{\eta}_2\boldsymbol{\eta}_2} \end{bmatrix}, \tag{8}$$

where $\boldsymbol{\eta} \in \mathbb{R}^N, \boldsymbol{\eta}_1 \in \mathbb{R}^n, \mathbf{J}_{\boldsymbol{\eta}_1\boldsymbol{\eta}_1} \in \mathbb{R}^{n\times n}, \mathbf{J}_{\boldsymbol{\eta}_1\boldsymbol{\eta}_2} \in \mathbb{R}^{n\times(N-n)}$, *and* $\mathbf{J}_{\boldsymbol{\eta}_2\boldsymbol{\eta}_2} \in \mathbb{R}^{(N-n)\times(N-n)}$ *with* $n < N$, *then the EFIM [4] of the parameter of interest* $\boldsymbol{\eta}_1$ *is given by* $\mathbf{J}_{\boldsymbol{\eta}_1}^{\mathrm{e}} = \mathbf{J}_{\boldsymbol{\eta}_1\boldsymbol{\eta}_1} - \mathbf{J}_{\boldsymbol{\eta}_1\boldsymbol{\eta}_2}\mathbf{J}_{\boldsymbol{\eta}_2\boldsymbol{\eta}_2}^{-1}\mathbf{J}_{\boldsymbol{\eta}_1\boldsymbol{\eta}_2}^{\mathrm{T}}$.

Using Definition 2, the EFIM of the parameter vector $\boldsymbol{\eta}$ is computed for different parameters of interest. For example, the EFIM when the parameter of interest is $\boldsymbol{\zeta} = [\boldsymbol{p}_U, \Phi_U]^{\mathrm{T}}$ is $\mathbf{J}_{\boldsymbol{\zeta}}^{\mathrm{e}} \in \mathcal{R}^{6\times 6}$. Here, the nuisance parameter is the complex path gain.

IV. Results

In this section, we use numerical simulations to find out which combinations of position and orientation parameters can be estimated - a parameter, $\boldsymbol{\zeta}$, can be estimated if the corresponding EFIM, $\mathbf{J}_{\boldsymbol{\zeta}}^{\mathrm{e}}$, is positive definite [4]. We also provide numerical position error bound (PEB) and orientation error bound (OEB) results for the case in which the source orientation and destination position are the unknown parameters. Our simulation framework consists of a source whose centroid is located at $\boldsymbol{p}_B = [1.5, 1.0, 4.0]^{\mathrm{T}}$ with the orientation angles $\boldsymbol{\Phi}_B = [1.1, 2.2, 0.7]^{\mathrm{T}}$. The position vectors are in meters, and the orientation vectors are in radians. The source has $N_B = 100$ antennas and the following number of transmit beams are considered $N_D \in [16, 32, 48, 64]^{\mathrm{T}}$. For each simulation, $T = 20$ symbols are transmitted, and the beamforming matrix $\boldsymbol{F}_t \in \mathcal{C}^{N_B\times N_D}$ changes during each of the T transmit symbols. The rows of this beamforming matrix are selected from a discrete Fourier transform-based (DFT) codebook. The destination is located at $\boldsymbol{p}_U = [2.6, 2.15, 5.1]^{\mathrm{T}}$ with the orientation angles $\boldsymbol{\Phi}_U = [0.1, 0.2, 0.1]^{\mathrm{T}}$. The Fraunhofer distance indicates that the destination is experiencing near-field propagation. The incorrect case when the far-field model is applied in this near-field simulation setup is termed "far-field." The correct case when the near-field model is used is termed "near-field."

With this simulation setup, we generate Table I[3]. This table highlights different combinations of the source and destination location that can be estimated. The "not applicable" term is used to highlight the fact that the parameter is known. When the term 3D is used, it means that the 3D version of that parameter can be estimated, and if the 3D version of the parameter can be estimated, all lower dimensions can also be estimated. As evident in Table I, it is impossible to estimate either the 3D position coordinates or the 3D orientation angles with only the signal from the line of sight (LOS) path when the far-field model is incorrectly applied to the near-field setup. However, if the near-field setup is correctly applied, estimating the 3D position coordinates or the 3D orientation angles are feasible with the LOS signal even without a beamforming matrix. While a 2D estimation of the source or destination's orientation angles is feasible when the far-field model is used and $N_U > 1$, it is important to note that estimating the source orientation angles is only possible in the far-field with beamforming (see Appendix A). This is in contrast with the near-field setup in which the estimation of the source's orientation angles is possible even with no beamforming provided that $N_U > 1$. In Figs. 2a and 2b, we present the PEB and OEB as a function of varying numbers of receive antennas[4]. Also, in these figures, the term "FF" is used to distinguish the incorrect case when the far-field model is applied to the study from the case when the near-field model is correctly applied to the study. As expected, the spherical wavefront in the near-field model results in more accurate localization. From the figures, the spherical wavefront is more advantageous for the estimation of the orientation.

V. Conclusion

This paper has examined the estimation of different combinations of a single-source and single destination's position and orientation. Through a study of the FIM, we have shown that while the source or destination's 3D orientation can be jointly estimated with the source or destination's 3D position in the near-field propagation regime, only the source or destination's 2D orientation can be jointly estimated with the source or destination's 2D position in the far-field propagation regime. Also, while without beamforming in the near-field, the source's 3D orientation can be estimated, the source's 2D orientation angles can not be estimated without beamforming in the far-field. Finally, a simulation of the PEB and OEB

[3]It is also important to note that the far-field simulation results, which are 2D, used to generate the far-field section in Table I, are generated by considering the first two components of the 3D position vector. Likewise, the 2D orientations (far-field simulation results presented in Table I) are the yaw and pitch out of the yaw, pitch, and roll - the first two components of the 3D orientation vector. .

[4]The PEB curves using both the near-field and far-field models are generated by considering the first two components of the 3D position vector. Also, for Fig. 2b in the revised manuscript, the OEB curves are generated by considering the yaw out of the yaw, pitch, and roll - the first component of the 3D orientation vector.

Table I
LOCATION ESTIMATION POSSIBILITIES WITH NEAR AND FAR FIELD MODELS. N/A INDICATES THE PARAMETER IS KNOWN. THE TERMS 3D AND 2D INDICATE THE DIMENSIONS IN WHICH THE PARAMETER CAN BE ESTIMATED IN THE PROPAGATION REGIMES.

	Near-field				Far-field			
Unknown Parameters	$\boldsymbol{p}_U$	$\boldsymbol{\Phi}_U$	$\boldsymbol{p}_B$	$\boldsymbol{\Phi}_B$	$\boldsymbol{p}_U$	$\boldsymbol{\Phi}_U$	$\boldsymbol{p}_B$	$\boldsymbol{\Phi}_B$
Source position and source orientation	N/A	N/A	3D	3D	N/A	N/A	2D	2D
Source position and destination orientation	N/A	3D	3D	N/A	N/A	2D	2D	N/A
Destination position and source orientation	3D	N/A	N/A	3D	2D	N/A	N/A	2D
Source position	N/A	N/A	3D	N/A	N/A	N/A	2D	N/A
Source orientation	N/A	N/A	N/A	3D	N/A	N/A	N/A	2D
Destination position	3D	N/A	N/A	N/A	2D	N/A	N/A	N/A
Destination orientation	N/A	3D	N/A	N/A	N/A	2D	N/A	N/A

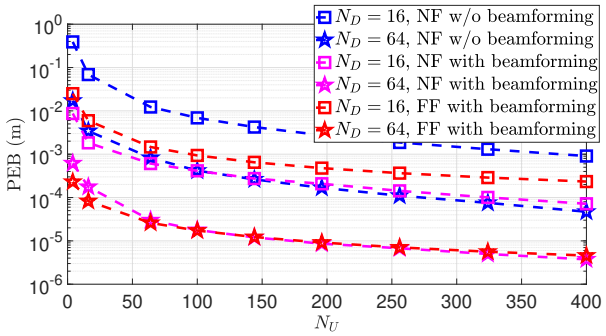

(a)

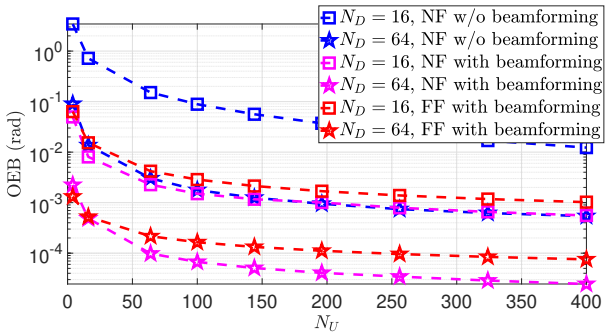

(b)

Figure 2. PEB and OEB in the near-field and far-field vs. N_U (2D simulation setup).

shows that the spherical information present in the near-field is much more useful for estimating orientation information.

APPENDIX

A. Analysis of Joint Estimation of $[\boldsymbol{\Phi}_B, \boldsymbol{\beta}]$ under the Far-Field Model

We start the proof by dropping the subscript t and using the identity beamforming matrix across the T transmissions. The FIM, $\mathbf{J}_{\boldsymbol{\Phi}_B}$, under the parameterization $\boldsymbol{\eta} = [\boldsymbol{\Phi}_B, \boldsymbol{\beta}]^{\mathrm{T}}$, is obtained by using the appropriate first derivatives in Definitions (1), and it has the following structure

$$\mathbf{J}_{\boldsymbol{\eta}} = \begin{bmatrix} \mathbf{J}_{\boldsymbol{\Phi}_B} & \mathbf{J}_{[\boldsymbol{\Phi}_B,\beta_{\mathrm{R}}]} & \mathbf{J}_{[\boldsymbol{\Phi}_B,\beta_{\mathrm{I}}]} \\ \mathbf{J}^{\mathrm{T}}_{\boldsymbol{\Phi}_R,\beta_R} & \mathbf{J}_{\beta_R} & 0 \\ \mathbf{J}^{\mathrm{T}}_{\boldsymbol{\Phi}_R,\beta_I} & 0 & \mathbf{J}_{\beta_I} \end{bmatrix},$$

and the EFIM can be written as

$$\mathbf{J}^{\mathrm{e}}_{\boldsymbol{\Phi}_B} = \mathbf{J}_{\boldsymbol{\Phi}_B} - [\mathbf{J}_{\beta_R}]^{-1}\mathbf{J}_{[\boldsymbol{\Phi}_B,\beta_{\mathrm{R}}]}\mathbf{J}^{\mathrm{T}}_{[\boldsymbol{\Phi}_B,\beta_{\mathrm{R}}]} + \mathbf{J}_{[\boldsymbol{\Phi}_B,\beta_{\mathrm{I}}]}\mathbf{J}^{\mathrm{T}}_{[\boldsymbol{\Phi}_B,\beta_{\mathrm{I}}]}, \tag{9}$$

and $\mathbf{J}^{\mathrm{e}}_{\boldsymbol{\Phi}_B} = \mathbf{J}_{\boldsymbol{\Phi}_B} - [\mathbf{J}_{\beta_R}]^{-1}\mathbf{J}_{\beta_R}\mathbf{J}_{\boldsymbol{\Phi}_R}$, the second equation results from noticing $\mathbf{J}_{\beta_R}\mathbf{J}_{\boldsymbol{\Phi}_R} = \mathbf{J}_{[\boldsymbol{\Phi}_B,\beta_{\mathrm{R}}]}\mathbf{J}^{\mathrm{T}}_{[\boldsymbol{\Phi}_B,\beta_{\mathrm{R}}]} + \mathbf{J}_{[\boldsymbol{\Phi}_B,\beta_{\mathrm{I}}]}\mathbf{J}_{[\boldsymbol{\Phi}_B,\beta_{\mathrm{I}}]}$. The proof follows as $\mathbf{J}^{\mathrm{e}}_{\boldsymbol{\Phi}_B} = 0$. Hence, with no beamforming, the source orientation can not be estimated with the far-field propagation model.

REFERENCES

[1] A. Shahmansoori, G. E. Garcia, G. Destino, G. Seco-Granados, and H. Wymeersch, "Position and orientation estimation through millimeter-wave MIMO in 5G systems," *IEEE Trans. on Wireless Commun.*, vol. 17, no. 3, pp. 1822–1835, Mar. 2018.

[2] Z. Abu-Shaban, X. Zhou, T. Abhayapala, G. Seco-Granados, and H. Wymeersch, "Error bounds for uplink and downlink 3D localization in 5G millimeter wave systems," *IEEE Trans. on Wireless Commun.*, vol. 17, no. 8, pp. 4939–4954, Aug. 2018.

[3] D.-R. Emenonye, H. S. Dhillon, and R. M. Buehrer, "Fundamentals of RIS-aided localization in the far-field," accepted to *IEEE Trans. on Wireless Commun., available online: arxiv.org/abs/2206.01652*, 2022.

[4] ——, "RIS-aided localization under position and orientation offsets in the near and far field," accepted to *IEEE Trans. on Wireless Commun., available online: arxiv.org/abs/2210.03599*, 2022.

[5] A. Elzanaty, A. Guerra, F. Guidi, and M.-S. Alouini, "Reconfigurable intelligent surfaces for localization: Position and orientation error bounds," *IEEE Trans. on Signal Processing*, vol. 69, pp. 5386–5402, Aug. 2021.

[6] R. Zekavat and R. M. Buehrer, *Handbook of Position Location: Theory, Practice and Advances*. John Wiley & Sons, 2011, vol. 27.

[7] M. Banagar and H. S. Dhillon, "Fundamentals of wobbling and hardware impairments-aware air-to-ground channel model," *accepted to IEEE Trans. on Wireless Commun., available online: arxiv.org/abs/2205.10957*, 2022.

[8] R. Mendrzik, H. Wymeersch, G. Bauch, and Z. Abu-Shaban, "Harnessing NLOS components for position and orientation estimation in 5G millimeter wave MIMO," *IEEE Trans. on Wireless Commun.*, vol. 18, no. 1, pp. 93–107, Jan. 2019.

[9] G. Naddafzadeh-Shirazi, M. B. Shenouda, and L. Lampe, "Second order cone programming for sensor network localization with anchor position uncertainty," *IEEE Trans. on Wireless Commun.*, vol. 13, no. 2, pp. 749–763, Feb. 2014.

[10] Y. Kim, B. Lee, H. So, and S.-C. Kim, "Localization technique considering position uncertainty of reference nodes in wireless sensor networks," *IEEE Sensors Journal*, vol. 18, no. 3, pp. 1324–1332, Dec. 2018.

[11] M. Angjelichinoski, D. Denkovski, V. Atanasovski, and L. Gavrilovska, "SPEAR: Source position estimation for anchor position uncertainty reduction," *IEEE Commun. Letters*, vol. 18, no. 4, pp. 560–563, 2014.

[12] ——, "Cramér–rao lower bounds of rss-based localization with anchor position uncertainty," *IEEE Trans. on Info. Theory*, vol. 61, no. 5, pp. 2807–2834, Mar. 2015.

[13] S. M. LaValle, *Planning Algorithms*. Cambridge University Press, 2006.